MITSUBISHI ELECTRIC RESEARCH LABORATORIES
http://www.merl.com

A dCDD-Based Transmit Diversity for NOMA Systems

Kim, Kyeong Jin; Liu, Hongwu; Lei, Hongjiang; Ding, Zhiguo; Orlik, Philip V.; Poor, H. Vincent

TR2020-070 June 09, 2020

Abstract

In this paper, a new transmit diversity scheme for cooperative non-orthogonal multiple access (NOMA) is proposed without perfect channel state information at the transmitter (CSIT). To support two users under a near-far user pairing constraint, a distributed cyclic delay diversity (dCDD) scheme is adjusted into NOMA by dividing a set of remote radio heads (RRHs) into two groups for multiple cyclic-prefixed single carrier transmissions. Using only a limited channel relevant information needed to make dCDD work, a new RRH assignment and power allocation mechanism is proposed. After then, closed-form expressions for the rates of two users achieved by the proposed RRH assignment and power allocation mechanism are derived. For various scenarios, link-level simulations verify that superior rates can be achieved by NOMA with dCDD over the traditional orthogonal multiple access with dCDD.

IEEE International Conference on Communications (ICC)

A dCDD-Based Transmit Diversity for NOMA Systems

Kyeong Jin Kim, Hongwu Liu, Hongjiang Lei, Zhiguo Ding, Philip V. Orlik, and H. Vincent Poor

***Abstract*—In this paper, a new transmit diversity scheme for cooperative non-orthogonal multiple access (NOMA) is proposed without perfect channel state information at the transmitter (CSIT). To support two users under a near-far user pairing constraint, a distributed cyclic delay diversity (dCDD) scheme is adjusted into NOMA by dividing a set of remote radio heads (RRHs) into two groups for multiple cyclic-prefixed single carrier transmissions. Using only a limited channel relevant information needed to make dCDD work, a new RRH assignment and power allocation mechanism is proposed. After then, closed-form expressions for the rates of two users achieved by the proposed RRH assignment and power allocation mechanism are derived. For various scenarios, link-level simulations verify that superior rates can be achieved by NOMA with dCDD over the traditional orthogonal multiple access with dCDD.**

***Index Terms*—Distributed cyclic delay diversity, NOMA, cyclic-prefixed single carrier transmission, near-far user pairing, rate.**

I. Introduction

To meet a high spectral efficiency, ultra-reliability, and low-latency required by tactile Internet, mobile edge computing, and beyond fifth generation (B5G) networks, non-orthogonal multiple access (NOMA) has emerged as a key technique for the upcoming decade of wireless communication evolution [1], [2]. With the aid of superposition coding in the power-domain, multiple users are multiplexed on the same time-frequency resource block with different power levels. To mitigate intra-cluster interference inherited from NOMA principles, successive interference cancellation (SIC) is in general applied at the receiver to recover the signals [3].

To enhance system performance and provide new degrees of freedom (DoF), various diversity techniques have been applied to NOMA, including multiple-input multiple-output (MIMO) antennas techniques and cooperative relaying schemes. Compared to conventional MIMO orthogonal multiple access (OMA), MIMO-NOMA can achieve a larger diversity order while serving severing more users [4]. It has been shown in [4] and [5] that channel gain disparity affects the diversity order achieved by NOMA users. To achieve full diversity for NOMA systems, transmit power allocation was proposed in [6]. To avoid the sophisticated channel ordering required by SIC, MIMO-NOMA was decomposed into single-input single-output (SISO) NOMA with a greatly decreased complexity [3]. However, power allocation and user ordering in MIMO-NOMA systems make the system performance evaluation more challenging over that of SISO-NOMA systems [7]. By sorting the users according to quality of service (QoS) requirements, the impact of relay selection schemes on performance of cooperative NOMA systems was investigated in [8] and [9], where two-stage relay selection protocols were proposed for cooperative NOMA systems with fixed power allocation and adaptive power allocation, respectively. The results showed that diversity gain for the two-stage decode-and-forward (DF) relaying scheme is proportional to the number of relays. The same results were obtained in [10], where the users were ordered by channel conditions.

In contrast to existing work, our main contributions can be summarized as follows.

- To achieve the transmit diversity gain without perfect channel state information at the transmitter (CSIT), the distributed cyclic delay diversity (dCDD) scheme [11], [12] is employed among spatially distributed central unit (CU), remote radio heads (RRHs), and two users. Furthermore, to support the near-far user pairing for NOMA [13], the original dCDD scheme is adjusted as follows to transmit two information signals simultaneously.
  - The CU divides a set of available RRHs into two groups based on the channel magnitudes, so that two users need to feed back a channel relevant information to the CU. This makes the CU control each group to transmit its own information signal to two users simultaneously. Thus, the proposed transmission scheme is different from the existing NOMA scheme that transmits the superposed signal.
  - For two separate groups, the CU allocates a different power to support the near-far user pairing.
- Due to different geographical locations of two users, non-identical frequency selective fading channels from RRHs to two users are considered. Over realistic and challenging channels, we provide an analytical framework jointly taking into account a different degree of RRH cooperation via dCDD protocol and power allocation.

A. Notation

$\mathbb{C}$ denotes the set of complex numbers; $\boldsymbol{I}_{m\times n}$ denotes the $m \times n$ matrix of ones; and $\mathbf{0}_{m\times n}$ denotes the $m \times n$ zero matrix. $\mathcal{CN}\left(\mu, \sigma^2\right)$ denotes the circularly symmetric complex

K. J. Kim and P. V. Orlik are with Mitsubishi Electric Research Laboratories (MERL), Cambridge, MA, USA.

H. Liu is with Shandong Jiaotong University, Jinan, China.

H. Lei is with Chongqing University of Posts and Telecommunications, Chongqing, China.

Z. Ding is with The University of Manchester, Manchester, UK.

H. V. Poor is with the Department of Electrical Engineering, Princeton University, Princeton, NJ, USA.

This work was supported in part by the U.S. National Science Foundation under Grants CCF-0939370 and CCF-1513915.

Gaussian distribution with mean μ and variance σ^2; $F_\varphi(\cdot)$ and $f_\varphi(\cdot)$, respectively, denote the cumulative distribution function (CDF) and probability density function (PDF) of the random variable (RV) φ; and $\binom{n}{k} \triangleq \frac{n!}{(n-k)!k!}$ denotes the binomial coefficient. Cardinalities of a vector $\boldsymbol{a}$ and a list $\mathbb{S}$ are respectively denoted by $|\boldsymbol{a}|$ and $|\mathbb{S}|$. In addition, subscripts are used to identify an element from a particular set. For a set of continuous random variables, $\{x_1, x_2, \ldots, x_N\}$, $x_{\langle i \rangle}$ denotes the ith largest random variable. For the order statistics, $\{x_{\langle 1 \rangle}, \ldots, x_{\langle N \rangle}\}$, we define the spacing statistics by the set $\{y_1, \ldots, y_N\}$, each of which is defined with $y_1 = x_{\langle 1 \rangle}$ and $y_k = x_{\langle k \rangle} - x_{\langle k-1 \rangle}$ for $2 \leq k \leq K$, so that we have $x_{\langle k \rangle} = \sum_{i=1}^{k} y_i$.

II. System and Channel Model

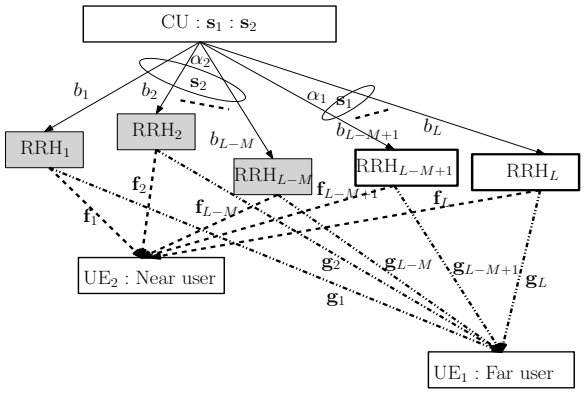

Fig. 1. Illustration of the proposed dCDD-based cooperative NOMA system with L RRHs and two users, UE_1 and UE_2.

Fig. 1 illustrates a block diagram of the cooperative NOMA system, which comprises a single CU, L RRHs, and two users, i.e., UE_1 and UE_2. The set of RRHs, $\{\mathrm{RRH}_i\}_{i=L-M+1}^{L}$, appears as the first group. Similarly another set of RRHs, $\{\mathrm{RRH}_i\}_{i=1}^{L-M}$, appears as the second group. Only one antenna is assumed to be deployed at each of the two users and RRHs due to hardware and power constraints. It is assumed that UE_1 is farther away than UE_2 from the RRHs, so that UE_1 appears as a far user in the considered system. For this cooperative and distributed system, the CU specifies how to control L RRHs [11] via dedicated highly reliable backhauls [14], $\{b_l\}_{l=1}^{L}$. The CU forms two independent data signals, $\boldsymbol{s}_1$ and $\boldsymbol{s}_2$ being transmitted simultaneously to UE_1 and UE_2. Half-duplex constraint is assumed for all the users and RRHs.

As a transmit diversity, dCDD is employed [11], [12]. It has been known that the maximum number of RRHs for dCDD is limited by the transmission symbol block size[1] and the maximum number of multipath components over channels connected from L RRHs to UE_1 and UE_2. Thus, this paper investigates only a finite-sized cooperative NOMA system comprising a finite number of L RRHs for full dCDD operation and two users. By employing appropriate channel sounding schemes or channel reciprocity [15], we further assume that each user is able to know the maximum number of multipath components of the channels connected to itself. Since the considered system employs intersymbol interference (ISI)-free cyclic-prefixed single carrier (CP-SC) transmissions [16], [17], each user needs to feed back the maximum number of multipath components of the channels connected to itself.

The following channels are assumed in the proposed system.

- Channels from L RRHs to UE_1 and UE_2: The multipath channels from the mth RRH to UE_1 and UE_2 are respectively given by
$$\boldsymbol{g}_m = \sqrt{(d_{1,m})^{-\epsilon_\mathrm{L}}}\tilde{\boldsymbol{g}}_m \text{ and } \boldsymbol{f}_m = \sqrt{(d_{2,m})^{-\epsilon_\mathrm{L}}}\tilde{\boldsymbol{f}}_m \quad (1)$$
where $\tilde{\boldsymbol{g}}_m$ and $\tilde{\boldsymbol{f}}_m$ identify the mth frequency selective fading channel with $N_{g,m} \triangleq |\tilde{\boldsymbol{g}}_m|$ and $N_{f,m} \triangleq |\tilde{\boldsymbol{f}}_m|$ multipath components. The distances from the mth RRH to UE_1 and UE_2 are respectively given by $d_{1,m}$ and $d_{2,m}$. The path loss exponent over channels $\boldsymbol{g}_m$ and $\boldsymbol{f}_m$, assumed to be identical, is denoted by ϵ_L. In addition, we assume that $d_{1,m} \neq d_{1,n}$ and $d_{2,m} \neq d_{2,n}, \forall m, n$.
- The multipath components of all frequency selective fading channels are assumed to be independent and identically distributed (i.i.d.) according to $\mathcal{CN}(0,1)$. However, due to different distances from L RRHs to UE_1 and UE_2, a composite frequency selective fading channel comprising small and large-scale fading is distributed independently but non-identically distributed (i.n.i.d.) in the whole system.

A. Summary of dCDD for CP-SC transmissions

1) Limited information fed back by UE_1 *and* UE_2*:*

- Without perfect CSIT of the channels connected to UE_1 and UE_2, it is necessary to compute the maximum number of multipath components, that is, $N_{g,\mathrm{CP}} \triangleq \max(\{N_{g,m}\}_{m=1}^{L})$ and $N_{f,\mathrm{CP}} \triangleq \max(\{N_{f,m}\}_{m=1}^{L})$. Based on them, the CU first computes N_CP as $N_\mathrm{CP} \triangleq \max(N_{g,\mathrm{CP}}, N_{f,\mathrm{CP}})$. After then, the CU computes the number of RRHs for dCDD as $K = \lfloor B/N_\mathrm{CP} \rfloor$, where $\lfloor \cdot \rfloor$ denotes the floor function. Due to an assumption of an underpopulated distributed system, the considered system has $L \leq K$.
- The channel magnitude of $\hat{\boldsymbol{g}}_m$ estimated by UE_1 is given by $\lambda_m \triangleq \|\hat{\boldsymbol{g}}_m\|^2$. Due to very reliable channel estimation made by UE_1, we assume $\hat{\boldsymbol{g}}_m \approx \boldsymbol{g}_m, \ \forall m$. For available L channel estimates, UE_1 arranges them as follows: $0 < \lambda_{\langle 1 \rangle} \leq \cdots \leq \lambda_{\langle L \rangle} < \infty$. After then it feeds back a list, $\mathbb{X}_g \triangleq [\langle 1 \rangle, \langle 2 \rangle, ..., \langle L \rangle]$, specifying channel magnitudes arranged in an ascending order. Based on N_CP and $\mathbb{X}_g$, the CU can divide the whole RRHs into two groups, after then apply CDD delays.

B. dCDD for CP-SC-NOMA Transmissions

Considering that UE_1 and UE_2 are respectively far and near users [13], more transmit power should be allocated to the signal of UE_1 according to the NOMA principal. To

[1]Since CP-SC transmission is used in the considered system, transmission symbols $\boldsymbol{s}_1$ and $\boldsymbol{s}_2$ are composed of B modulated symbols.

meet these heterogeneous constraints and considering only L available RRHs, we modify dCDD as follows:

- Based on $\mathbb{X}_g$, the CU divides L RRHs into two groups. The first group composed of M RRHs, and indexed by the set $\mathbb{S}_1 \triangleq [\langle L-M+1\rangle, \ldots, \langle L\rangle] \subset \mathbb{X}_g$, transmits $\boldsymbol{s}_1$. Similarly, the second group, composed of the remaining $(L-M)$ RRHs, transmits $\boldsymbol{s}_2$. The second group is indexed by the set $\mathbb{S}_2 \triangleq [\langle 1\rangle, \ldots, \langle L-M\rangle] \triangleq \mathbb{X}_g - \mathbb{S}_1$.
- Since $\mathbb{S}_2$ is determined by the CU based on the channel connected to UE_1, it should be shared with UE_2.

Having applied dCDD, the received signal at UE_1 is given by

$$\boldsymbol{r}_1 = \sqrt{\alpha_1 P_s} \sum_{m=L-M+1}^{L} (d_{1,\langle m\rangle})^{-\epsilon_{\mathrm{L}}/2} \tilde{\boldsymbol{G}}_{\langle m\rangle} \tilde{\boldsymbol{s}}_{1,m} + \left[\sqrt{\alpha_2 P_s} \sum_{m=1}^{L-M} (d_{1,\langle m\rangle})^{-\epsilon_{\mathrm{L}}/2} \tilde{\boldsymbol{G}}_{\langle m\rangle} \tilde{\boldsymbol{s}}_{2,m}\right]_{J_1} + \boldsymbol{z}_1 \quad (2)$$

where P_s is the peak transmission power at all the RRHs, and $\tilde{\boldsymbol{G}}_{\langle m\rangle}$ denotes the right circulant channel matrix determined by $\tilde{\boldsymbol{g}}_{\langle m\rangle}$. The additive noise over all the channels is denoted by $\boldsymbol{z}_1 \sim \mathcal{CN}(\boldsymbol{0}, \sigma_z^2 \boldsymbol{I}_B)$. In addition, α_1 and $\alpha_2 \triangleq 1-\alpha_1$ respectively denote power allocation coefficients for UE_i in transmitting $\boldsymbol{s}_i$. The mth transformed block symbols $\tilde{\boldsymbol{s}}_{1,m}$ and $\tilde{\boldsymbol{s}}_{2,m}$ are defined as $\tilde{\boldsymbol{s}}_{1,m} \triangleq \boldsymbol{P}_{\Delta_m} \boldsymbol{s}_1$ and $\tilde{\boldsymbol{s}}_{2,m} \triangleq \boldsymbol{P}_{\Delta_{\tilde{m}}} \boldsymbol{s}_2$, where $m \in \mathbb{S}_1$ and $\tilde{m} \in \mathbb{S}_2$. The permutation shifting matrices $\boldsymbol{P}_{\Delta_m} \in \mathbb{C}^{B\times B}$ and $\boldsymbol{P}_{\Delta_{\tilde{m}}} \in \mathbb{C}^{B\times B}$ can be obtained from the identity matrix $\boldsymbol{I}_B$ by respectively circularly shifting down by Δ_m and $\Delta_{\tilde{m}}$. Note that $[\cdot]_{J_1}$ is the interfering signal at UE_1.

With the use of permutation matrices, we rewrite (2) as follows:

$$\boldsymbol{r}_1 = \sqrt{\tilde{\alpha}_1} \sum_{m=L-M+1}^{L} (d_{1,\langle m\rangle})^{-\epsilon_{\mathrm{L}}/2} \tilde{\boldsymbol{G}}_{\langle m\rangle} \boldsymbol{P}_{\Delta_m} \boldsymbol{s}_1 + \sqrt{\tilde{\alpha}_2} \sum_{m=1}^{L-M} (d_{1,\langle m\rangle})^{-\epsilon_{\mathrm{L}}/2} \tilde{\boldsymbol{G}}_{\langle m\rangle} \boldsymbol{P}_{\Delta_{\tilde{m}}} \boldsymbol{s}_2 + \boldsymbol{z}_1 \quad (3)$$

where $\tilde{\alpha}_1 \triangleq \alpha_1 P_s$ and $\tilde{\alpha}_2 \triangleq \alpha_2 P_s$. In addition, $\tilde{\boldsymbol{G}}_{\langle m\rangle} \boldsymbol{P}_{\Delta_m}$ and $\tilde{\boldsymbol{G}}_{\langle m\rangle} \boldsymbol{P}_{\Delta_{\tilde{m}}}$ are right circulant matrices.

Similar to (3), the received signal at UE_2 is given by

$$\boldsymbol{r}_2 = \sqrt{\tilde{\alpha}_1} \sum_{m \in \mathbb{S}_1, |\mathbb{S}_1|=M} (d_{2,m})^{-\epsilon_{\mathrm{L}}/2} \tilde{\boldsymbol{F}}_m \boldsymbol{P}_{\Delta_m} \boldsymbol{s}_1 + \sqrt{\tilde{\alpha}_2} \sum_{\substack{m \in \mathbb{S}_2, \\ |\mathbb{S}_2|=L-M}} (d_{2,m})^{-\epsilon_{\mathrm{L}}/2} \tilde{\boldsymbol{F}}_m \boldsymbol{P}_{\Delta_{\tilde{m}}} \boldsymbol{s}_2 + \boldsymbol{z}_2 \quad (4)$$

where we assume that $\boldsymbol{z}_2 \sim \mathcal{CN}(\boldsymbol{0}, \sigma_z^2 \boldsymbol{I}_B)$. Since $\tilde{\boldsymbol{F}}_m$, determined by $\tilde{\boldsymbol{f}}_m$, is right circulant, $\tilde{\boldsymbol{F}}_m \boldsymbol{P}_{\Delta_m}$ and $\tilde{\boldsymbol{F}}_m \boldsymbol{P}_{\Delta_{\tilde{m}}}$ are right circulant matrices as well. From (3) and (4), we can extract the following facts:

- The order statistics are related to large-scale and small-scale fading, and the CDD delay assignment for UE_1, so that it is necessary to use them in analyzing the performance of UE_1.
- The selection mechanism for $\mathbb{S}_1$ and $\mathbb{S}_2$ will be crucial in achieving the rates of UE_1 and UE_2 under the near-far user pairing constraint. However, the CU has only N_{CP}, $\mathbb{X}_g$, $\mathbb{S}_1$, and $\mathbb{S}_2$ for controlling the RRHs by the dCDD protocol.

III. Performance Analysis of CP-SC-NOMA Transmissions with dCDD

UE_2 first decodes $\boldsymbol{s}_1$, after then decodes $\boldsymbol{s}_2$. According to (4), the receive SNR in decoding $\boldsymbol{s}_1$ is given by

$$\gamma_{2,\boldsymbol{s}_1} = \frac{\alpha_1 P_s \sum_{m \in \mathbb{S}_1, |\mathbb{S}_1|=M} \|\boldsymbol{f}_m\|^2}{\alpha_2 P_s \sum_{m \in \mathbb{S}_2, |\mathbb{S}_2|=L-M} \|\boldsymbol{f}_m\|^2 + \sigma_z^2} \quad (5)$$

where we have assumed that $E\{\boldsymbol{s}_j\} = \boldsymbol{0}$ and $E\{\boldsymbol{s}_j(\boldsymbol{s}_j)^H\} = \boldsymbol{I}_B$, for $j = 1, 2$. In addition, $E\{\boldsymbol{s}_i(\boldsymbol{s}_j)^H\} = \boldsymbol{I}_B \delta_{i-j'}$ with the Kronecker delta function, $\delta_l = \begin{cases} 0 & \text{if } l \neq 0 \\ 1 & \text{if } l = 0. \end{cases}$ After then, assuming $\boldsymbol{s}_1$ is perfectly decoded, UE_2 decodes $\boldsymbol{s}_2$, so that the SNR in decoding $\boldsymbol{s}_2$ is given by

$$\gamma_{2,\boldsymbol{s}_2} = \alpha_2 \sum_{m \in \mathbb{S}_2, |\mathbb{S}_2|=L-M} \|\tilde{\boldsymbol{f}}_m\|^2 / \beta_{2,m} \quad (6)$$

where $1/\beta_{2,m} \triangleq P_S (d_{2,m})^{-\epsilon_{\mathrm{L}}} / \sigma_z^2$. Based on (6), the PDF of $\gamma_{2,\boldsymbol{s}_2}$ is given by

$$f_{\gamma_{2,\boldsymbol{s}_2}}(x) = \sum_{\substack{i_3 \in \mathbb{S}_2, \\ |\mathbb{S}_2|=L-M}} \sum_{j_3=1}^{L_{g,i_3}} \frac{\theta_{L,L-M}(i_3, j_3)}{\Gamma(j_3)(\alpha_2)^{j_3}} (x)^{j_3-1} e^{-\frac{\beta_{2,i_3} x}{\alpha_2}}$$

where $\theta_{L,L-M}(i_3, j_3)$ denotes the partial fraction coefficients. According to (3), the SNR for decoding $\boldsymbol{s}_1$ by UE_1 is given by

$$\gamma_{1,\boldsymbol{s}_1} = \frac{\alpha_1 C_{\max}^{L,M}}{\alpha_2 D_{\min}^{L,L-M} + 1} \quad (7)$$

where $C_{\max}^{L,M} \triangleq \sum_{m=L-M+1}^{L} \|\tilde{\boldsymbol{g}}_{\langle m\rangle}\|^2 / \beta_{1,\langle m\rangle}$, $D_{\min}^{L,L-M} \triangleq \sum_{m=1}^{L-M} \|\tilde{\boldsymbol{g}}_{\langle m\rangle}\|^2 / \beta_{1,\langle m\rangle}$, and $1/\beta_{1,\langle m\rangle} \triangleq \rho (d_{1,\langle m\rangle})^{-\epsilon_{\mathrm{L}}}$. From (7), we can see that in contrast to the expression for $\gamma_{2,\boldsymbol{s}_1}$, the order statistics are involved in the expression for $\gamma_{1,\boldsymbol{s}_1}$. In addition, due to the use of the order statistics, $C_{\max}^{L,M}$ and $D_{\min}^{L,L-M}$ are correlated with each other. From these challenging difficulties, it is necessary to derive their PDFs. We first derive the PDFs of $C_{\max}^{L,M}$ and $D_{\min}^{L,L-M}$ in the following *Corollary 1*.

Corollary 1: Denote $Y_k \triangleq \|\tilde{\boldsymbol{g}}_{\langle k\rangle}\|^2 / \beta_{1,\langle k\rangle}$ the kth smallest instantaneous SNR. Using the spacing statistics [18], [19], alternative forms for $C_{\max}^{L,M}$ and $D_{\min}^{L,L-M}$ can be derived, which are uncorrelated with each other. Then, we can compute the target PDFs as follows:

$$f_{D_{\min}^{L,L-M}}(x) = \sum_{\min} \sum_{i_3=1}^{L-M} \sum_{j_3=1}^{\nu_{i_3}+1} \frac{E_{\min^{L,L-M}}(i_3, j_3)}{\Gamma(j_3)} e^{-\xi_{j_3} x} x^{j_3-1},$$

$$f_{C_{\max}^{L,M}}(x) = \sum_{\max} \sum_{i_4=1}^{M} \sum_{j_4=1}^{\mu_{i_4}+1} \frac{E_{\max^{L,M}}(i_4, j_4)}{\Gamma(j_4)} e^{-\zeta_{i_4} x} x^{j_4-1} \quad (8)$$

where unspecified terms, $\sum_{\max}$, $\sum_{\min}$, $\{\xi_{j_3}s, \nu_{j_3}s\}$, and $\{\zeta_{j_4}s, \mu_{j_4}s\}$ are defined in Appendix A. In addition, $E_{\min^{L,L-M}}(\cdot,\cdot)$ and $E_{\max^{L,M}}(\cdot,\cdot)$ denote partial fraction coefficients.

Proof: See Appendix A. ∎

Based on (8), the PDF of $\gamma_{1,\boldsymbol{s}_1}$ can be derived as (9), provided at the top of the next page.

A. Analysis for Achievable Rate

a) Achievable rate of UE_2*:* The achievable rate of UE_2 is given by

$$R_{2,(L-M)} = \int_0^\infty \log_2(1+x) f_{\gamma_{2,\boldsymbol{s}_2}}(x)dx. \tag{10}$$

$$R_{2,(L-M)} = \frac{1}{\log(2)} \sum_{i_3 \in \mathbb{S}_2, |\mathbb{S}_2|=L-M} \sum_{j_3=1}^{L_{g,i_3}} \frac{\theta_{L,L-M}(i_3,j_3)}{\Gamma(j_3)(\alpha_2)^{j_3}} \left(\frac{\beta_{2,i_3}}{\alpha_2}\right)^{-j_3} G_{3,2}^{1,3}\left(\frac{\beta_{2,i_3}}{\alpha_2}\middle| \begin{matrix} 1-j_3, 1, 1 \\ 1, 0 \end{matrix}\right) \tag{11}$$

where the Laplace transform of a particular Meijer G-function [20, eq. (07.34.22.0003.01)], [21, eq. (2.24.3.1)] is used for the derivation.

b) Achievable rate of UE_1*:* The achievable rate of UE_1 is provided in the following *Theorem 1*.

Theorem 1: The dCDD-based CP-SC-NOMA transmission provides UE_1 with the rate provided by (12), which is provided at the top of the next page.

Proof: See Appendix B. ∎

In (12), $G_{p_1,q_1:p_2,q_2:p_3,q_3}^{m_1,0:m_2,n_2:m_3:n_3}\left(x,y\middle| \begin{matrix} \cdot \\ \cdot \end{matrix}\middle| \begin{matrix} \cdot \\ \cdot \end{matrix}\middle| \begin{matrix} \cdot \\ \cdot \end{matrix}\right)$ denotes the generalized bivariate Meijer G-function [20, eq. (07.34.21.0081.01)] and [22].

IV. Simulations

We assume the following simulation setting.

- For CP-SC transmissions, we assume that $B = 32$ and $N_{\mathrm{CP}} = 6$. Thus, the CU can support up to five RRHs for dCDD.
- Five RRHs are placed at $\{(0,12), (-12,12), (-3,12), (-9,12), (-16.9145, 6.1564)\}$ in a 2-D plane. When $L < 5$ RRHs are selected for dCDD, we choose the first L RRHs for the simulations.
- The two users, UE_1 and UE_2, are respectively placed at $(3,-3)$ and $(-3,3)$.
- According to [23], we assume that $\epsilon_{\mathrm{L}} = 2.09$.
- We consider a non-identical number of multipath components and a non-identical distance between two nodes in the system. Thus, non-identical frequency selective fading is assumed for all the channels in the system.
- We use a fixed $P_s = 1$ for the whole link-level simulations.

The curves obtained via link-level simulations are denoted by **Ex**, whereas analytically obtained performance curves are denoted by **An**.

Since the derivation of a closed-form expression for $R_{1,(L,M)}$, expressed by (12), is challenging in the proposed system, we first verify its accuracy comparing with the corresponding exact rate provided in Fig. 2. The corresponding rate of UE_2 is provided in Fig. 3.

For various combinations of (L,M), α_1, α_2, and $(N_{f,m}, N_{g,m})$, Figs. 2 and 3 show that (12) and (11) provide accurate analysis for the rates of UE_1 and UE_2.

A. Rate analysis

a) The impact of the cardinality of $\mathbb{S}_1$*:* We use a fixed $\alpha_1 = 0.9$ and $\{N_{g,m}\}_{m=1}^{L} = 2$ to investigate the impact of the cardinality of set $\mathbb{S}_1$ on the rate. In Fig. 4, we use fixed $|\mathbb{S}_1| = 2$ and $|\mathbb{S}_1| = 3$ for two values of L. This figure shows that at a fixed $|\mathbb{S}_1|$, more RRHs in $\mathbb{S}_1$ results in greater rate up to a certain SNR. However, in the high SNR region, an asymptotic rate advantage is determined by the ratio of $|\mathbb{S}_1|$ to L. Thus, we can see that $R_{1,(4,3)} > R_{1,(5,3)}$. Similar results can be seen with $|\mathbb{S}_1| = 2$, i.e., $R_{1,(4,2)} > R_{1,(5,2)}$. Form these observations, a greater $|\mathbb{S}_1|$ does not guarantee a greater rate in the asymptotic SNR region.

b) The impact of power allocation to RRHs specified by $\mathbb{S}_1$ *and* $\mathbb{S}_2$*:* For four RRHs and $|\mathbb{S}_1| = 3$, we investigate the impact of α_1 on the rate of UE_1 and UE_2 in Fig. 5. In this scenario, only one RRH out of four RRHs is used to transmit $\boldsymbol{s}_2$. This figure shows that as α_1 increases, UE_1 achieves a greater rate, whereas UE_2 achieve a lower rate since less power is allocated to RRHs specified by $\mathbb{S}_2$. This figure also shows that $R_{2,(L-M)}$ increases as the SNR increases, whereas $R_{1,(L,M)}$ is upper bounded by its limit since $\gamma_{1,\boldsymbol{s}_1}$ is approximated by $\gamma_{1,\boldsymbol{s}_1} \approx \frac{\alpha_1 C_{\max}^{L,M}}{\alpha_2 D_{\min}^{L,L-M}}$ as the SNR increases. That is, UE_1 enters the interference-limited region. From these observations, the sum rate is like a double-edged sword. If the pair of (L,M) and the power allocation are not properly handled, the sum of rate will be dominated by UE_2, which violates the near-far user pairing constraint. Since the CU knows only $\mathbb{X}_g$ and controls α_1, every pair of (L,M) is not possible to meet this constraint. For $|\mathbb{S}_1| = 2$, i.e., two RRHs are assigned to transmit $\boldsymbol{s}_2$, we can see distinctive results in Fig. 6 comparing with those of Fig. 5. For the considered scenario, $(L=4, M=2, \alpha_1 = 0.6)$ and $(L=4, M=2, \alpha_1 = 0.7)$ are not feasible user pairs. Although other pairs $(L=4, M=2, \alpha_1 = 0.8)$ and $(L=4, M=2, \alpha_1 = 0.9)$ are feasible, they have limited operating SNR ranges to support the near-far user pairing. These observations suggest the following RRH assignment and power allocation mechanism:

- A larger $|\mathbb{S}_1|$ results in $R_{1,(L,M)} > R_{2,(L-M)}$, so that it is necessary to assign more RRHs to transmit $\boldsymbol{s}_1$.
- Due to the existence of the interfering signal at UE_1, the CU needs to assign more transmit power to the RRHs specified by $\mathbb{S}_1$.

c) Comparison with OMA with dCDD: For various system parameters, Figs. 3 and 4 show that NOMA with dCDD achieves superior rate comparing with OMA with dCDD for both users.

V. Conclusions

In this paper, we have proposed a new transmit diversity scheme for the two-user CP-SC NOMA system. To support the

$$f_{\gamma_{1,\boldsymbol{s}_1}}(x)=\sum_{\max}\sum_{i_4=1}^{M}\sum_{j_4=1}^{\mu_{i_4}+1}\sum_{\min}\sum_{i_3=1}^{L-M}\sum_{j_3=1}^{\nu_{i_3}+1}\frac{E_{\max^{L,M}}(i_4,j_4)}{\Gamma(j_4)}\frac{E_{\min^{L,L-M}}(i_3,j_3)}{\Gamma(j_3)}$$
$$\Big(\frac{1}{\alpha_1}\Big)^{j_4}\sum_{l=0}^{j_4}\binom{j_4}{l}(\alpha_2)^l\Gamma(l+j_3)e^{-\frac{\zeta_{i_4}}{\alpha_1}x}x^{j_4-1}\Big(\frac{\alpha_2\zeta_{i_3}}{\alpha_1}x+\xi_{j_3}\Big)^{-j_3-l}. \quad (9)$$

$$R_{1,(L,M)}=\frac{1}{\log(2)}\sum_{\max}\sum_{i_4=1}^{M}\sum_{j_4=1}^{\mu_{i_4}+1}\sum_{\min}\sum_{i_3=1}^{L-M}\sum_{j_3=1}^{\nu_{i_3}+1}\frac{E_{\max^{L,M}}(i_4,j_4)}{\Gamma(j_4)}\frac{E_{\min^{L,L-M}}(i_3,j_3)}{\Gamma(j_3)}$$
$$\Big(\frac{1}{\alpha_1}\Big)^{j_4}\sum_{l=0}^{j_4}\binom{j_4}{l}(\alpha_2)^l\Gamma(l+j_3)(\alpha_2)^{-l-j_3}\Big(\frac{\zeta_{i_4}}{a_1}\Big)G^{1,0:1,2:1,1}_{1,0:2,2:1,1}\Big(\frac{\zeta_{i_3}}{\alpha_1},\frac{\xi_{j_3}}{\alpha_2}\Big|\begin{array}{c}1\\\cdot\end{array}\Big|\begin{array}{c}j_4,j_4\\j_4,j_4-1\end{array}\Big|\begin{array}{c}1-l-j_3\\0\end{array}\Big). \quad (12)$$

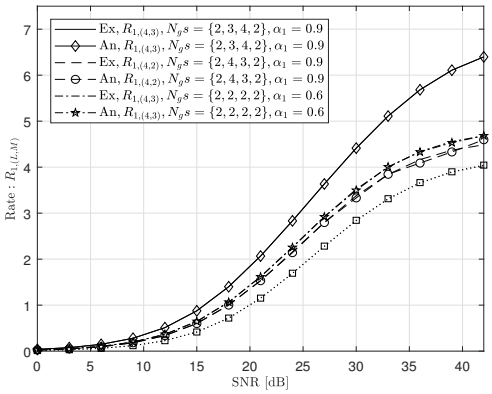

Fig. 2. Achievable rate of UE_1 for various system parameters.

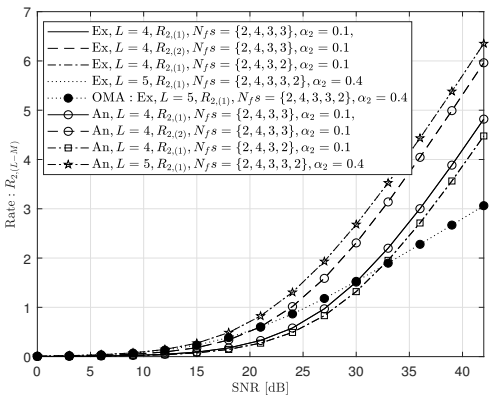

Fig. 3. Achievable rate of UE_2 for various system parameters.

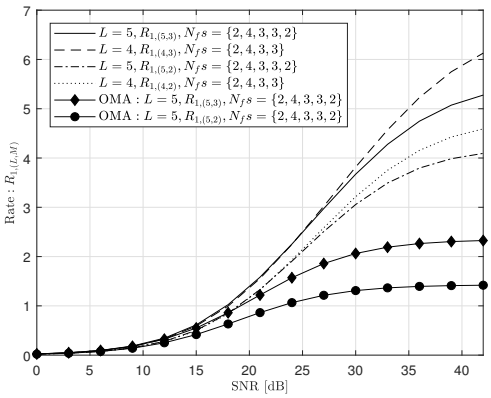

Fig. 4. Achievable rate of UE_1 for various pairs of (L, M).

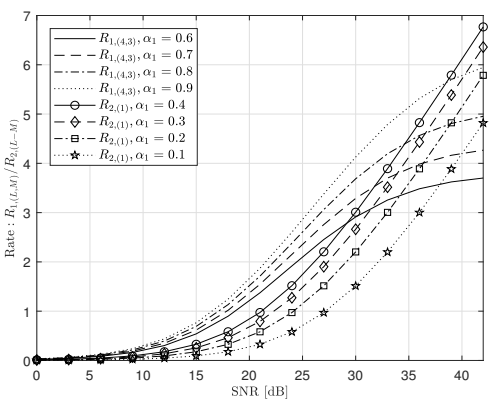

Fig. 5. Achievable rate of UE_1 and UE_2 for various values of α_1 with $N_{g,m} = N_{f,m} = \{2,4,3,3\}$, $L = 4$, and $|\mathbb{S}_1| = 3$.

near-far user pairing, a new joint RRH assignment and power allocation mechanism for dCDD based CP-SC transmissions without requiring perfect CSIT of the whole channels at the CU has been proposed. For i.n.i.d. frequency selective fading channels, new closed-form expressions for the rates of two users have been derived. Its accuracy has also been verified. By link-level simulations, it has been shown that every pair of (L, M) is not supported for the whole range of power allocation for the CP-SC NOMA system due to the near-far user pairing constraint.

APPENDIX A: DERIVATION OF *Corollary 3*

Let $\tilde{\lambda}_{\langle m\rangle}$ be defined by $\tilde{\lambda}_{\langle m\rangle} \triangleq \|\tilde{\boldsymbol{g}}_{\langle m\rangle}\|^2/\beta_{1,\langle m\rangle}$.

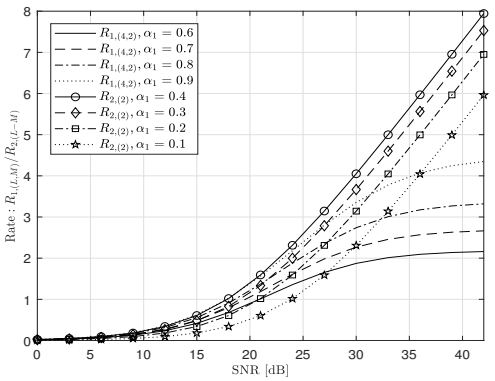

Fig. 6. Achievable rate of UE_1 and UE_2 for various values of α_1 with $N_{g,m} = N_{f,m} = \{2, 4, 3, 3\}$, $L = 4$, and $|\mathbb{S}_1| = 2$.

a) PDF of $D_{\min}^{L,L-M}$: The joint PDF of $Y_1 \triangleq \tilde{\lambda}_{\langle 1 \rangle}, \ldots, Y_{L-M} \triangleq \tilde{\lambda}_{\langle L-M \rangle}$ can be written as

$$f_{Y_1,Y_2,\ldots,Y_{L-M}}(y_1, y_2, \ldots, y_{L-M}) = \frac{1}{M!}\mathrm{Per}(\boldsymbol{A}_{\min}^{L,L-M}) \quad \text{(A.1)}$$

where the permanent matrix, $\mathrm{Per}(\boldsymbol{A}_{\min}^{L,L-M})$, is defined as follows:

$$\boldsymbol{A}_{\min}^{L,L-M} = \begin{bmatrix} f_{Y_1}(y_1) & \cdots & f_{Y_1}(y_{L-M}) & \tilde{F}_{Y_1}(y_{L-M}) \\ \vdots & \vdots & \vdots & \\ f_{Y_L}(y_1) & \cdots & f_{Y_L}(y_{L-M}) & \tilde{F}_{Y_L}(y_{L-M}) \\ \underbrace{\quad 1 \quad} & \underbrace{\quad 1 \quad} & \underbrace{\quad 1 \quad} & \underbrace{\quad M \quad} \end{bmatrix}$$

where $\tilde{F}_{Y_k}(y_k)$ and $f_{Y_k}(y_k)$ are the complementary CDF (CCDF) and PDF of Y_k, i.e., the kth smallest SNR. Their expressions are given by

$$\tilde{F}_{Y_k}(y_k) = \frac{\gamma_l(N_{g,k}, \beta_{1,k} y_k)}{\Gamma(N_{g,k})} \text{ and}$$
$$f_{Y_k}(y_k) = \frac{(\beta_{1,k})^{N_{g,k}}}{\Gamma(N_{g,k})} e^{-\beta_{1,k} y_k} (y_k)^{N_{g,k}-1} \quad \text{(A.2)}$$

where $\gamma_l(\cdot,\cdot)$ denotes the lower incomplete gamma function. Furthermore, $\begin{bmatrix} \underbrace{\boldsymbol{a}_1}_{i} & \underbrace{\boldsymbol{a}_2}_{j} \end{bmatrix}$ denotes i copies of $\boldsymbol{a}_1$ and j copies of $\boldsymbol{a}_2$. The moment generating function (MGF) of $D_{\min}^{L,L-M}$ can be defined as

$$M_{D_{\min}^{L,L-M}}(s) = \int_0^\infty \int_{y_1}^\infty \cdots \int_{y_{L-M-2}}^\infty \int_{y_{L-M-1}}^\infty I_{\min}^{L,L-M}(s) dy_{L-M} \ldots dy_2 dy_1$$

where $I_{\min}^{L,L-M}(s)$ is given by

$$I_{\min}^{L,L-M}(s) = \frac{1}{(M)!} e^{-s(\sum_{j=1}^{L-M} y_j)} \mathrm{Per}(\boldsymbol{A}_{\min}^{L,L-M}). \quad \text{(A.3)}$$

Having applied spacing, that is, $Y_k = \sum_{l=1}^{k} X_k$, $M_{D_{\min}^{L,L-M}}(s)$ can be evaluated as (A.4), provided at the top of the next page. In (A.4), we have defined $\beta_j = \beta_{1,j}$, $C_1 = \prod_{j=1}^{L-M} \frac{(\beta_{n_j})^{m_{n_j}}}{\Gamma(m_{n_j})}$, $C_2 = \prod_{j=L-M+1}^{L} (\beta_{n_j})^{l_j}/\Gamma(l_j+1)$, $\tilde{m}_{\min} = \sum_{j=L-M+1}^{L} l_j + m_{n_{L-M}} - 1$, and $\tilde{\beta}_{\min} = \sum_{j=L-M}^{L} \beta_{n_j}$. In addition, $C_3 \triangleq (L-M)^{-\nu_1-1}(L-M-1)^{-\nu_2-1} \ldots 2^{-\nu_{L-M-1}-1}\Gamma(\nu_1+1)\Gamma(\nu_2+1)\ldots\Gamma(\nu_{L-M-1}+1)\Gamma(\nu_{L-M}+1)$, $\xi_i = \frac{1}{(L-M-i+1)}\sum_{j=i}^{L} \beta_{n_j}$, $\nu_i = \begin{cases} m_{n_1} - 1 + \sum_{j=2}^{L-M} p_{j,i} & \text{for } i = 1 \\ \sum_{j=i}^{L-M} p_{j,i} & \text{for } 2 \le i \le L-M, \end{cases}$ $\sum_{\substack{p_{J,1},\ldots,p_{J,a} \\ \sum_{i_J=1}^{a} p_{J,i} = b}}$ denotes the sum of positive integer indices $\{p_{J,1}, \ldots, p_{J,a}\}$ satisfying $\sum_{i=1}^{a} p_{J,i} = b$. After applying the partial fraction to A_1 in (A.4), and the inverse MGF, the PDF can be derived as follows:

$$f_{D_{\min}^{L,L-M}}(t) = \sum_{\min} \sum_{i=1}^{L-M} \sum_{j=1}^{\nu_i+1} \frac{E_{\min}{}^{L,L-M}(i,j)}{\Gamma(j)} e^{-\xi_j t} t^{j-1}. \quad \text{(A.5)}$$

b) PDF of $C_{\max}^{L,M}$: The joint PDF of $Y_{L-M+1} \triangleq \tilde{\lambda}_{\langle L-M+1 \rangle}, \ldots, Y_L \triangleq \tilde{\lambda}_{\langle L \rangle}$ can be written as

$$f_{Y_{L-M+1},\ldots,Y_L}(y_1, y_2, \ldots, y_M) = \frac{1}{(L-M)!}\mathrm{Per}(\boldsymbol{A}_{\max}^{L,M}) \quad \text{(A.6)}$$

where the permanent matrix, $\mathrm{Per}(\boldsymbol{A}_{\max}^{L,M})$, is determined as follows:

$$\boldsymbol{A}_{\max}^{L,M} \triangleq \begin{bmatrix} F_1(y_1) & f_1(y_1) & \cdots & f_1(y_M) \\ \vdots & \vdots & \vdots & \vdots \\ F_L(y_1) & f_L(y_1) & \cdots & f_L(y_M) \\ \underbrace{\quad L-M \quad} & \underbrace{\quad 1 \quad} & \underbrace{\quad 1 \quad} & \underbrace{\quad 1 \quad} \end{bmatrix} \quad \text{(A.7)}$$

where $F_k(\cdot) = 1 - \tilde{F}_k(\cdot)$ denotes the CDF of Y_k. The MGF of $C_{\max}^{L,M}$ can be defined as

$$M_{C_{\max}^{L,M}}(s) = \int_0^\infty \int_{y_1}^\infty \cdots \int_{y_{M-2}}^\infty \int_{y_{M-1}}^\infty I_{\max}^{L,M}(s) dy_M \ldots dy_1$$

where $I_{\max}^{L,M}(s)$ is given by

$$I_{\max}^{L,M} = \frac{1}{(L-M)!} e^{-s(\sum_{j=1}^{M} y_j)} \mathrm{Per}(\boldsymbol{A}_{\max}^{L,M}). \quad \text{(A.8)}$$

After some manipulations, $M_{C_{\max}^{L,M}}(s)$ is given by (A.9) provided on the next page. In (A.9), we have defined $D_1 \triangleq \prod_{j=1}^{M} \frac{(\beta_{n_j})^{m_{n_j}}}{\Gamma(m_{n_j})}$, $\tilde{k}_l \triangleq \sum_{t=0}^{m_{n_l}-1} t k_{l,t+1}$, $\tilde{m}_{\max} \triangleq m_{n_1} - 1 + \sum_{l=M+1}^{L} \tilde{k}_l$, and $D_2 \triangleq \left(\prod_{j=M+1}^{L} C_{q_j}\right)$ with $C_{q_j} = \sum_{q_j=0}^{1} \binom{1}{q_j} (-1)^{q_j} \sum_{\substack{k_{j,1},\ldots,k_{j,m_{n_j}} \\ k_{j,1}+\ldots+k_{j,m_{n_j}}=1}} \frac{\prod_{t=0}^{m_{n_j}-1} \frac{(\beta_{n_j})^{k_{j,t+1}}}{(t!)}}{k_{j,1}! \cdots q_{k,m_{n_j}}!}$. In addition, $\zeta_i = \begin{cases} \frac{(\sum_{j=1}^{M} \beta_{n_j} + \sum_{j=M+1}^{L} \beta_{n_j} q_j)}{M} & \text{for } i = 1 \\ \frac{\sum_{j=i}^{M} \beta_{n_j}}{(M-i+1)} & \text{for } 2 \le i \le M \end{cases}$, $\mu_i = \begin{cases} \tilde{m}_{\max} + \sum_{j=2}^{M} q_{j,1} & \text{for } i = 1 \\ \sum_{j=i}^{M} p_{j,i} & \text{for } 2 \le i \le M \end{cases}$, $D_3 = (M)^{-\mu_1-1}(M-1)^{-\mu_2-1} \ldots 2^{-\mu_{M-1}-1}\Gamma(\mu_1+1)\ldots\Gamma(\mu_M+1)$. Thus,

$$M_{D_{\min}^{L,L-M}}(s) = \sum_{\substack{n_1,\ldots,n_{L-M} \\ n_1\neq n_2\neq\ldots\neq n_{L-M}}} C_1 \sum_{l_{L-M+1}=0}^{m_{n_{L-M+1}}-1} \cdots \sum_{l_L=0}^{m_{n_L}-1} C_2 \sum_{\substack{p_{2,1},p_{2,2} \\ \sum_{i_2=1}^{2} p_{2,i_2}=m_{n_2}-1}} \frac{\Gamma(m_{n_2})}{\prod_{i=1}^{2} p_{2,i}!}\cdots$$
$$\sum_{\substack{p_{L-M,1},\cdots,p_{L-M,L-M} \\ \sum_{i_{L-M}=1}^{L-M} p_{L-M,i}=\tilde{m}_{\min}}} \frac{\Gamma(\tilde{m}_{\min}+1)}{\prod_{i=1}^{L-M} p_{L-M,i}!} C_3 \prod_{i=1}^{L-M}\Big((s+\xi_i)^{-\nu_i-1}\Big) = \sum_{\min} \underbrace{\prod_{i=1}^{L-M}\Big((s+\xi_i)^{-\nu_i-1}\Big)}_{A_1}. \tag{A.4}$$

$$M_{C_{\max}^{L,M}}(s) = \sum_{\substack{n_1,\ldots,n_M \\ n_1\neq n_2\neq\ldots\neq n_M}} D_1 D_2 \sum_{\substack{p_{2,1},p_{2,2} \\ p_{2,1}+p_{2,2}=m_{n_2}-1}} \frac{\Gamma(m_{n_2})}{\prod_{i=1}^{2} p_{2,i}!} \sum_{\substack{p_{3,1},p_{3,2},p_{3,3} \\ p_{3,1}+p_{3,2}+p_{3,3}=m_{n_3}-1}} \frac{\Gamma(m_{n_3})}{\prod_{i=1}^{3} p_{3,i}!}\cdots$$
$$\sum_{\substack{p_{M,1},\ldots,p_{M,M} \\ p_{M,1}+\ldots+p_{M,M}=m_{n_M}-1}} \frac{\Gamma(m_{n_M})}{\prod_{i=1}^{M} p_{M,i}!} D_3\Big(\prod_{i=1}^{M}(s+\zeta_i)^{-\mu_i-1}\Big) = \sum_{\max} \underbrace{\Big(\prod_{i=1}^{M}(s+\zeta_i)^{-\mu_i-1}\Big)}_{A_2}. \tag{A.9}$$

after applying the partial fraction to A_2 and then the inverse MGF, the PDF can be derived as follows:

$$f_{C_{\max}^{L,M}}(t) = \sum_{\max}\sum_{i=1}^{M}\sum_{j=1}^{\mu_i+1} \frac{E_{\max^{L,M}}(i,j)e^{-\zeta_i t}t^{j-1}}{\Gamma(j)}. \tag{A.10}$$

Appendix B: Derivation of *Theorem 1*

The rate, $R_{1,(M,L-M)}$, is given by

$$R_{1,(M,L-M)} = \int_0^\infty \log_2(1+x) f_{\gamma_{1,s_1}}(x)dx. \tag{B.1}$$

To compute (B.1), we first express the following functions of x in terms of meijer-G functions:

$$\log_2(1+x)x^{j_4-1} = \frac{1}{\log(2)} G_{2,2}^{1,2}\Big(x\Big|\begin{matrix} j_4, j_4 \\ j_4, j_4-1\end{matrix}\Big),$$
$$e^{-\frac{\zeta_{i_4}}{\alpha_1}x} = G_{0,1}^{1,0}\Big(\frac{\zeta_{i_4}}{\alpha_1}x\Big|\begin{matrix}\cdot \\ 0\end{matrix}\Big), \text{ and}$$
$$\Big(\frac{\alpha_2\zeta_{i_3}}{\alpha_1}x+\xi_{j_3}\Big)^{-j_3-l} = G_{1,1}^{1,1}\Big(\frac{\alpha_2\zeta_{i_3}}{\alpha_1\xi_{j_3}}x\Big|\begin{matrix}1-l-j_4 \\ 0\end{matrix}\Big)(\xi_{j_3})^{-l-j_3}.$$

Having applied [24], we can derive (12).

References

[1] L. Dai, *et al.*, "Non-orthogonal multiple access for 5G: solutions, challenges, opportunities, and future research trends," *IEEE Commun. Magazine*, pp. 74–81, Sep. 2015.

[2] Z. Ding, *et al.*, "Application of non-orthogonal multiple access in LTE and 5G networks," *IEEE Commun. Magazine*, pp. 185–191, Feb. 2017.

[3] ——, "A survey on non-orthogonal multiple access for 5G networks: Research challenges and future trends," *IEEE J. Sel. Areas Commun.*, vol. 35, no. 10, pp. 2181–2195, Oct. 2017.

[4] Z. Ding, F. Adachi, and H. V. Poor, "The application of MIMO to non-orthogonal multiple access," *IEEE Trans. Wireless Commun.*, vol. 15, no. 1, pp. 537–552, Jan. 2016.

[5] Z. Ding, P. Fan, and H. V. Poor, "Impact of user pairing on 5G non-orthogonal multiple-access downlink transmissions," *IEEE Trans. Veh. Technol.*, vol. 65, no. 8, pp. 6010–6023, 2016.

[6] E. Balevi, "Multiuser diversity gain in uplink NOMA," in *Proc. 2018 IEEE Vehicular Technology Conference (VTC-Fall)*, Chicago, IL, 27-30 Aug. 2018, pp. 1–5.

[7] Y. Liu, *et al.*, "Nonorthogonal multiple access for 5G and beyond," *Proc. IEEE*, vol. 105, no. 12, pp. 2347–2381, Dec. 2017.

[8] Z. Ding, H. Dai, and H. V. Poor, "Relay selection for cooperative NOMA," *IEEE Wireless Commun. Lett.*, vol. 5, no. 4, pp. 416–419, Aug. 2016.

[9] Z. Yang, Z. Ding, Y. Wu, and P. Fan, "Novel relay selection strategies for cooperative NOMA," *IEEE Trans. Veh. Technol.*, vol. 66, no. 11, pp. 10 114–10 123, 2017.

[10] P. Xu, Z. Yang, Z. Ding, and Z. Zhang, "Optimal relay selection schemes for cooperative NOMA," *IEEE Trans. Veh. Technol.*, vol. 67, no. 8, pp. 7851–7855, 2018.

[11] K. J. Kim, M. D. Renzo, H. Liu, P. V. Orlik, and H. V. Poor, "Performance analysis of distributed single carrier systems with distributed cyclic delay diversity," *IEEE Trans. Commun.*, vol. 65, no. 12, pp. 5514 – 5528, Dec. 2017.

[12] K. J. Kim, *et al.*, "Distributed cyclic delay diversity systems with spatially distributed interferers," *IEEE Trans. Wireless Commun.*, vol. 18, no. 4, pp. 2066 – 2079, Jun. 2019.

[13] H. Liu, Z. Ding, K. J. Kim, K. S. Kwak, and H. V. Poor, "Decode-and-forward relaying for cooperative NOMA systems with direct links," *IEEE Trans. Wireless Commun.*, vol. 12, pp. 8077–8093, Dec. 2018.

[14] K. J. Kim, T. Khan, and P. Orlik, "Performance analysis of cooperative systems with unreliable backhauls and selection combining," *IEEE Trans. Veh. Technol.*, vol. 66, no. 3, pp. 2448–2461, Mar. 2017.

[15] F. Gao, A. Nallanathan, and C. Tellambura, "Blind channel estimation for cyclic-prefixed single-carrier systems by exploiting real symbol characteristics," *IEEE Trans. Veh. Technol.*, vol. 56, no. 5, pp. 2487–2498, Sep. 2007.

[16] K. J. Kim, T. Q. Duong, and X. Tran, "Performance analysis of cognitive spectrum-sharing single-carrier systems with relay selection," *IEEE Trans. Signal Process.*, vol. 60, no. 12, pp. 6435–6449, Dec. 2012.

[17] K. J. Kim and T. A. Tsiftsis, "Performance analysis of QRD-based cyclically prefixed single-carrier transmissions with opportunistic scheduling," *IEEE Trans. Veh. Technol.*, vol. 60, no. 1, pp. 328–333, Jan. 2011.

[18] M.-S. Alouini and M. K. Simon, "An MGF-based performance analysis of generalized selection combining over Rayleigh fading channels," *IEEE Trans. Commun.*, vol. 48, no. 3, pp. 401 – 415, Mar. 2000.

[19] Y. Ma and C. C. Chai, "Unified error probability analysis for generalized selection combining in Nakagami fading channels," *IEEE J. Sel. Areas Commun.*, vol. 18, no. 11, pp. 2198–2210, Nov. 2000.

[20] Wolfman Research Inc. The Mathematical Functions Site. Accessed: Oct.13, 2019. [Online]. Available: http://functions.wolfman.com

[21] A. P. Prudnikov, Y. A. Brychkov, and O. I. Marichev, *Integral and Series. Vol. 3: More Special Functions*, 3rd ed. London: Gordon and Breach, 1992.

[22] I. Shafique, *et al.*, "A new formula for the BER of binary modulations with dual-branch selection over generalized-K composite fading channels," *IEEE Trans. Commun.*, vol. 59, no. 10, pp. 2654–2658, Oct. 2011.

[23] 3GPP, TR 36.828 (V11.0.0), "Further enhancements to lte time division duplex (TDD) for downlink-uplink (DL-UL) interference management and traffic adaptation," Jun. 2012.

[24] H. Chergui, M. Benjillali, and S. Saoudi, "Performance analysis of project-and-forward relaying in mixed MIMO-pinhole and Rayleigh dual-hop channel," *IEEE Commun. Lett.*, vol. 20, no. 3, pp. 610–613, Mar. 2016.